

Review on heart-rate estimation from photoplethysmography and accelerometer signals during physical exercise

Vijitha Periyasamy ¹, Manojit Pramanik ^{1*}, and Prasanta Kumar Ghosh ^{2*}

¹*School of Chemical and Biomedical Engineering, Nanyang Technological University, Singapore
637459,*

²*Electrical Engineering, Indian Institute of Science, Bangalore-560012*

vijitha@ntu.edu.sg, manojit@ntu.edu.sg, prasantg@ee.iisc.ernet.in

Abstract:

Non-invasive monitoring of physiological signals during physical exercise is essential to customize the exercise module. Photoplethysmography (PPG) signal has often been used to non-invasively monitor heart-rate, respiratory-rate, and blood-pressure among other physiological signals. Typically, PPG signal is acquired using pulse-oximeter from fingertip or wrist. Advantage of wrist based PPG sensors is that it is more convenient to wear. Other sensors such as accelerometer can also be integrated with it due to large area on the wrist. This article provides a review of the algorithms developed for heart rate estimation during physical exercise from the PPG signals and accelerometer signals. The datasets used to develop these techniques are described. Algorithms for denoising of PPG signals using accelerometer signals are either in time domain and frequency domain.

Index Terms: Heart-rate monitoring, spectral peak tracking, accelerometer signal, motion artifact, physical activity.

1 Introduction

Real-time heart rate (HR) estimation from the photoplethysmography (PPG) signals is a key step in developing wearable devices that can monitor the HR in a non-invasive way [1]. The PPG signal is obtained from pulse oximeters and its periodicity corresponds to the cardiac rhythm [2]. Oximeters are designed with a light source and detector placed either in reflection mode or in transmission mode [Fig. 1(a)]. Light of wavelength between 500 nm to 900 nm is illuminated on the skin. The light transmitted or reflected by the skin is proportional to the blood flow [Fig.1(b)] [3]. Blood flow in the vessels is mediated by the heart beat [Fig. 1(c)]. In spite of the HR information available in the PPG signal, reliable estimation of the HR is not straightforward due to the fact that the PPG signals are vulnerable to motion artifacts (MA), which strongly interfere with the HR. Fig. 1(d) shows a 3 seconds long PPG signal acquired when the subject is at rest and Fig. 1(e) shows the same when the subject is exercising on thread-mill. Figs. 1(f) and (g) are the respective tri-axial accelerometer data. In comparison, Electrocardiogram (ECG) signals shown in Figs. 1(h) and (i) are more robust to MA. MA in PPG during exercise is strong compared to the resting data. Depending on the type of physical activity of the user, the MA component can completely mask the HR information in the PPG signals causing the HR monitoring from the PPG signal challenging [4, 5]. Effective MA removal techniques are required for PPG signals acquired during physical exercise to accurately find the HR information. The steps involved in HR estimation using accelerometer information is shown in the block diagram [Fig. 1(j)].

A typical approach in estimating HR in the presence of MA is to first remove MA from the PPG signal. There are several techniques in the literature for removing MA from the PPG signal [6]. Some of these techniques do not require motion information from

an accelerometer while some others do. Independent Component Analysis (ICA) is one technique where motion data is not required; however, it requires multiple PPG sensors [7]. ICA has been proposed in both time-domain [8] and frequency-domain [9]. However, the assumption of statistical independence in ICA does not hold well in PPG signal contaminated by MA [10]. On the other hand, when the acceleration data is available, the MA component is adaptively cancelled from the PPG signal using an adaptive filter following least mean square (LMS) [11], normalized LMS [12, 13], fast transversal recursive least square (RLS) algorithms [14], as well as spectrum subtraction technique [15], and Laguerre basis function based signal representation [16]. Other MA-removal techniques include electronic processing methodology [17], time-frequency analysis [18], wavelet denoising [19, 20], higher order statistics [9], empirical mode decomposition [21, 22], and random forest based method [23] to name a few. However, in case of an intense physical exercise, most of these techniques do not work well [10]. Acceleration data has also been used for the observation model for Kalman filter [24] as well as for Kalman smoother [25] to remove MA. The acceleration data reflects the hand movement in 3-D space while MA in PPG signal also originates from other sources such as changes of the gap between skin and a pulse oximeters surface which cannot be corrected by using acceleration data.[10]

In contrast to the adaptive filtering [26], Zhilin *et al.* [10] has proposed a TROIKA (signal decomposiTiOn for denoising, sparse signal RecOnstructIon for high resolution spectrum estimation, and spectral peak trAcking) framework, where a high-resolution spectrum of the PPG signal is calculated using sparse signal reconstruction following signal decomposition using the singular spectrum analysis (SSA). Spectral peak tracking (SPT) is performed on the reconstructed PPG spectra to estimate the HR, which has been shown to be more accurate compared to other HR estimators. However, the SPT

solely depends on the initialization of the HR in the first frame. When a wrongly detected spectral peak is used for initialization, the entire estimated HR trajectory could be different from the actual HR trajectory.

Different MA cancellation algorithms such as adaptive noise cancellation (ANC) [27], Kalman filter (KF), Kalman smoother, as well as sparse reconstruction with SSA decomposition remove MA from the PPG signals to varying degrees. This depends on the nature of the MA cancellation algorithm, filter order and other chosen parameters. The extent of MA cancellation further affects the SPT based HR estimation performance.

Spectrum of the denoised signal was used to compute the HR [10]. The initialization of the HR in the first few spectras of the PPG signal is done by selecting the frequency corresponding to the highest intensity, since the periodicity of the PPG signals in the first few seconds correspond to HR. A window around the initialized HR is used to estimate the HR in future spectras. The window location is updated in each prediction. This leads to tracking of the HR in the successive spectras to lie within the given range of beats per minute(BPM).

In this review, pre-processing techniques are discussed. Pre-processing includes simple steps such as detrending and bandpass filtering. This is done to remove base-line drift and mask the PPG and accelerometer signal within 20 to 210 BPM [28]. Removal of MA from PPG using accelerometer signal is done in either time domain or frequency domain. Time domain algorithms include filtering techniques, whereas spectral subtraction is done in frequency domain. Different time domain and frequency domain algorithms developed for MA cancellation and advancements in SPT techniques are discussed. Datasets collected with subject on treadmill are detailed in the next section. The frequency and time domain algorithms developed on the dataset is detailed in section 3. Discussions and conclusion

is detailed in section 4 and 5, respectively.

2 Datasets

The extent of MA component in PPG signal is not measurable. Hence, comparing the efficiency of PPG denoising algorithms remain a challenge. To estimate the efficiency of MA cancellation algorithms, MA is added to the PPG signal which is termed as synthetic dataset [29]. Algorithms developed on synthetic data doesn't perform well on real-world data. Real-world datasets were acquired while subjects were on thread-mill [10]. Algorithms developed for clinical dataset is beyond the scope of this article [30].

2.1 Synthetic

Target PPG signal is mixed with MA in frequency domain [29]. PPG signal is obtained from a subject's finger-tip in resting state. Two MA signals are extracted from PPG sources using temporally constrained independent component analysis and adaptive filtering [31]. MA signals are added to PPG signals in a proportion. To find the efficiency of the synthesized signal, signal to noise ratio (SNR) is computed.

2.2 Real-world

Well-documented and open-source data was collected and used by Zhang *et al.*, [10]. The collected dataset consists of PPG, tri-axial accelerometer and electrocardiogram (ECG) signals [10]. All three signals were recorded simultaneously. Dataset 1 was collected from 10 male subjects under the age of 18 to 33. Pulse oximeter of wavelength 609 nm was embedded into a wrist band which also incorporated accelerometer. Single channel ECG was acquired from the chest. All the signals were sampled at 125 Hz. Signals

were acquired for 8 minutes on a treadmill. The first minute subject was at a speed of 2 *km/hr*, next minute the speed was 4 *km/hr*, then at a speed of 10 *km/hr* for a minute after which the speed was increased to 15-17 *km/hr* for 1-1.5 minute Fig. 2(a). Then the whole cycle was reversed for next 3.5 minutes. Subjects were requested to perform intentional movements such as wipe sweat and button the shirt in addition to free swinging of the arm.

Dataset 2 consists of two-channel PPG signals, both at wavelength 515 nm which was embedded into wrist band (which also has accelerometer) to collect the data from 12 subjects on treadmill. Each PPG data was acquired for 5 minutes. Subjects were at rest for first 30 seconds, then speed was 6 *km/hr* for 1 minute and 12 *km/hr* for the next minute after which the speed was slowed to 6 *km/hr* and then increased to 12 *km/hr* for 1 minute before resting for 30 second. For one of the subjects the speed was 8 *km/hr* and 15 *km/hr* Fig. 2(b). ECG signals were also collected during exercise and annotated for heart rate in beats per minute (BPM) over every 8 second time-window which overlapped by 6 seconds. The advanced dataset was made publicly available as a part of 2015 IEEE Signal Processing Cup (SPC) challenge. This review focusses on the HR estimation algorithms developed for SPC data¹ [10].

Third set of data was recorded using the set-up by Zhang *et al.*; from 8 subjects [32]. Seven subjects were healthy male, while the other female subject had abnormal heart rhythm and blood pressure. Female subject and 3 other subjects performed type 1 exercise which was forearm and upper arm exercise. 6 healthy subjects performed type 2 intense exercise such as boxing air. These 10 recordings were the test set to validate the algorithms by entrants of the challenge. The HR annotated from ECG is also available.

¹<http://www.zhilinzhang.com/spcup2015>

Dataset was developed by Peng *et al.*, with a different set of motions on treadmill. To estimate the efficiency of the MA removal techniques, PPG was acquired from right index finger during four different motions which are bending of finger at 90° , waving of hand, pressurizing probe clip and walking each for 20 seconds [29]. This data was collected from 18 males and 13 females. These activities were performed after 5 minutes of rest, using two pulse oximeters on each hand at a frequency of 200 Hz. The left hand was stationary on thread-mill during the acquisition at a speed of 5 *km/hr*.

3 Methods

During the rest state the periodicity in PPG signal corresponds to the heart beat. But this periodicity is disturbed when the motion artifact interferes. HR estimation, which is a three stage process, begins with band-pass filtering to remove the noise beyond the range of heart beat. The bandpass filtered signal is denoised to remove the motion artifact. Denoising techniques, which is dependent on accelerometer signals, vary from simple filtering to complex sparse reconstruction. Heart rate tracking is the crucial step. HR tracking is done in the frequency domain.

3.1 Pre-processing of PPG signal

PPG signal is band-pass filtered from 0.5 Hz and 8 Hz [29]. For SPC dataset, PPG signals and accelerometer signals are band-pass filtered from 0.4 Hz and 7 Hz. Usually HR varies from 40 BPM to 120 BPM, which corresponds to 0.6 Hz to 3.5 Hz [10]. Butterworth IIR filter was used [33]. This bandpass filtering increases the sparseness in the signals which is an advantage for sparsity based algorithms and reduces the wandering of HR tracks beyond range. Since PPG was prone to baseline drift due to electronic interference,

detrending and normalizations were also done as a part of preprocessing. [34].

3.2 Motion artifact removal and HR estimation

3.2.1 Frequency domain

TROIKA framework is robust to strong motion artifact [10]. Signal decomposition, sparse signal reconstruction (SSR), and spectral peak tracking (SPT) formed the basis [Fig. 2c]. For signal decomposition, the PPG signal is segmented into smaller, overlapping components. Singular spectrum analysis (SSA), single channel independent component analysis, and empirical mode decomposition are some of the techniques used in literature, SSA was used in TROIKA. This time domain decomposition involves embedding, singular value decomposition, grouping and reconstruction. Focal underdetermined system solver algorithm which is used in source localization and direction-of-arrival estimation was used for SSR. SPT involves initialization, peak selection, and trend verification. The verification is dependent on the characteristics of the recorded data and the nature of heart rate. TROIKA is also performed on signals down-sampled at 25 HZ.

TROIKA framework which was considered gold standard was modified for better accuracy [33]. SSA was followed by real-time clustering (RTC), frequency points selection and prediction followed by multiple-way selection. In the spectrum of denoised signal obtained after SSA, three peaks which were two-thirds the intensity of the maximum were retained. The selected peaks were clustered. Due to the smoothness in the HR, when the cluster of peaks are not close to the previous peak, the previous peak is considered for BPM calculation. BPM for the current frame (beyond first three frames) were dependent on the BPM of two previous HRs. In multiple-way selection, the previous computed HRs were corrected. TROIKA was the first algorithm to use singular spectrum analysis for

MA removal in PPG signals which was improvized further for better accuracy.

CARMA (closest subspace algorithm for reducing motion artifact) depends on singular value decomposition (SVD) of the Hankel matrix obtained after preprocessing the PPG and accelerometer signals [Fig. 2d] [35]. Key assumption of this technique was that the arifact and heart rate lie in different subspaces. Adative peak tracking was used for HR estimation. Spectrum subtraction is combined with ensemble empirical mode decomposition (EEMD). EEMD decomposes the PPG signal and acceleration signals into intrinsic mode functions [Fig. 2e] [36]. Spectrum subtraction is used to remove the spectrum of acceleration signal from PPG signal. In order to increase the resolution of the spectrum for better HR estimation, zero-padding Discrete Fourier Transformation (DFT) followed by KF for tracking of HR [37]. This technique doesn't require pre-processing, hence it is computationally simple. SPECTRAP algorithm has spectrum subtraction, peak tracking, and post-processing. The down-sampled signals were filtered and subjected to symmetric least square based spectral subtraction. MA spectrum is subtracted from PPG spectrum [38]. Cumulative spectrum (CUMSPEC) technique sparsifies the signal using iterative method adaptive thresholding, followed by median filtering of HR estimates. Genetic algorithm was used for HR tracking [39]. These algorithm were compared with TROIKA.

Gridless spectral Estimation and SVM based peak Selection (GRESS) is another algorithm for Zhang's advanced dataset [40]. The conventional estimation of HR in a spectrum which is pixelated is modified. Grid-less spectral estimation is dependent on sparsity of the signal. Peak-to-peak separation distance and amplitude peaks were used to train a two-class support vector machine [Fig. 3a]. Gridless spectral estimation helped to overcome the basis mismatch. Basis mismatch was observed in other algorithms which

assumed sparsely aligned to specific frequency grids. Spectral peak selection was formulated into a pattern classification task, hence user defined parameters were reduced. This algorithm performed better than TROIKA framework for few subjects, but was not as efficient as JOSS (joint sparse spectrum reconstruction). JOSS was once again proposed by Zhilin Zhang. Multiple measurement vector model was used for joint spectral analysis which was followed by spectral subtraction [41]. The peak verification process was intensified as compared to TROIKA [42]. After the peak verification steps of TROIKA, the peak discovery is incorporated which smooths the selected peak [Fig. 3b]. Instantaneous fundamental frequency of acceleration signal is computed using finite harmonic sum (HSUM) [Fig. 4a][3]. The computed fundamental frequency is fitted to the PPG signal, where one of the harmonic sums corresponds to the HR while the harmonics are of MA. In MC-SMD (Multi-channel spectral matrix decomposition) technique the spectra of PPG signal are divided by the spectrum of acceleration signal [Fig. 4b] [43]. This algorithm is compared with 25 Hz JOSS and TROIKA results. MC-SMD is computationally cheap because it does not have a noise-removal module. Short-time Fourier transform (SFST) and spectral analysis is also combined [44]. SFST was robust to frequency variation compared to wavelet transform techniques. Adding an average filter increased the HR estimation.

3.2.2 Time domain

Spectral peak search-comb filtering (SPS-CF) was developed which is dependent on the weighted sum of the delayed signal and band-pass time-domain signal [29]. The feed-forward comb filter was evenly spaced peaks in the magnitude frequency response. Adaptive filters were estimated for removal of MA from PPG signals [45]. The authors used

normalized least mean square (NLMS) filter to denoise each of the 2 PPG signals in advanced Zhang dataset. This leads to six denoised PPG signals. STFT of these signals were multiplied for a single spectrum. HR was estimated from the STFT spectrum by picking the highest intensity representing 40-170 BPM. To maintain the trend, the threshold was set for the chosen BPM. The efficiency of the adaptive filter technique is compared with TROIKA.

MISPT (Multiple Initialization spectral peak tracking) has an denoising technique based on adaptive noise cancellation filter and emphasis is laid on peak selection [Fig. 5a] [46]. FFT of denoised time-domain signal was taken for HR estimation. Initialization was done in each spectral window and the trajectory was generated by back tracking. The trajectory was based on selection of location of maximum intensity within a given window. The HR which corresponded to trajectory of maximum strength was the recorded BPM. This algorithm outperformed TROIKA and JOSS in both 25 Hz and 125 Hz PPG signal.

One of the three accelerometer signals are chosen based on their highest bandpower. The chosen accelerometer signal is used to filter the PPG signal using RLS filter [47]. Bandpass filtered signals were normalized and averaged [Fig. 5b] [48]. These averaged PPG signals and accelerometer signals are downsampled to 25 Hz. After which DFT is performed and Wiener filtering (WF) is applied to remove MA. To increase the HR estimation accuracy, phases of the chosen peak and the previous peaks are refined. Time varying spectral comparison of PPG acceleration signal enables the removal of peaks due to MA (SpaMA) [Fig. 5c] [49]. RLS filter and Blackman-Harris-Window was used as pre-processing steps to estimate HR in HEAL-T [Fig. 6a] [50]. MURAD- Multiple Reference Adaptive noise cancellation for HR estimation is the algorithm where the denoising of PPG using RLS filter is done individually by the three accelerometer signals and once

again by the signal obtained by difference between the two PPG signals [51]. RLS and spectral decomposition (SD) technique was combined for better performance [52]. The key of this algorithm was the use of Bayesian decision for HR estimation. This algorithm is compared with 25 Hz TROIKA results.

Result of NLMS algorithm was further bandpass filtered with discrete oscillator based adaptive notch filter (OSC-ANF) for instant tracking of changing frequency [Fig. 6b] [53]. HR estimation was done using recursive filtering after EEMD [54]. SVD is used for MA cancellation (MAC) and HR was estimated from denoised signal using spectral analysis [55]. Since MA is minimal for the first few seconds, HR estimation in the spectral domain is simple [41]. The frequency corresponding to the maximum spectral intensity converted to beats per minute (BPM) is the heart rate. A window is taken around the initial heart rate while estimation of the HR in the subsequent windows. This is based on the fact that rate of change of HR is gradual. The window location is adaptive over each spectral window to enable gradual rise or fall in the HR. The frequency of optimized spectral peak within the given denoised spectral window is the HR [29]. Estimated HR is also compensated for the directional trend of BPM.

4 Discussion

The results of the existing algorithms are tabulated in Table 1. Performance of both the domains across 12 subjects (dataset 2) are listed. Twelve frequency domain and twelve time domain algorithms are shown. Least error by frequency domain denoising techniques is 0.73 BPM and time domain is 0.97 BPM. Consistently, the error in HR estimation by all the algorithms for subject 10 is high. The only exception is HSUM technique [3].

Table 1: Comparison of the error in BPM across various algorithms detailed

-	Sub1	Sub2	Sub3	Sub4	Sub5	Sub6	Sub7	Sub8	Sub9	Sub10	Sub11	Sub12	Avg
Frequency domain	-	-	-	-	-	-	-	-	-	-	-	-	-
TROIKA(125) [10]	2.29	2.19	2.00	2.15	2.01	2.76	1.67	1.93	1.86	4.70	1.72	2.84	2.34
TROIKA(25) [10]	2.87	2.75	1.91	2.25	1.69	3.16	1.72	1.83	1.58	4.00	1.96	3.33	2.42
RTC [33]	1.70	2.36	1.00	2.14	0.87	1.96	1.01	0.73	0.86	8.93	1.15	1.88	2.05
CARMA [35]	2.58	1.48	1.40	2.47	1.54	3.24	1.01	1.19	0.93	6.28	1.68	3.30	2.26
EEMD [36]	2.06	3.59	0.92	1.54	0.97	1.64	2.25	0.63	0.62	4.62	1.30	1.80	1.83
DFT+KF [37]	2.11	1.89	1.01	1.08	0.61	1.66	0.54	0.59	0.54	4.12	1.15	2.83	1.51
SPECTRAP [38]	1.18	2.42	0.86	1.38	0.92	1.37	1.53	0.64	0.60	3.65	0.92	1.25	1.39
CUMSPEC [39]	1.81	1.44	0.63	1.16	0.83	1.40	1.02	0.63	0.68	2.77	1.03	0.90	1.19
GRESS [40]	1.18	2.42	0.86	1.38	0.76	1.37	0.72	0.64	0.60	3.65	0.82	1.04	1.45
JOSS [41]	1.33	1.75	1.47	1.48	0.69	1.32	0.71	0.56	0.49	3.81	0.78	1.04	1.28
HSUM [3]	0.61	0.76	0.65	0.59	0.53	0.52	0.59	0.51	0.41	0.58	1.48	1.58	0.73
MC+SMD [43]	1.16	1.07	0.80	1.13	0.98	1.29	0.88	0.81	0.55	3.18	0.79	0.72	1.11
SFST+SA [44]	1.23	1.51	1.19	0.92	0.61	0.78	0.48	0.49	0.58	3.00	0.73	1.24	1.06
Time domain	-	-	-	-	-	-	-	-	-	-	-	-	-
NLMS [45]	2.40	1.21	1.20	1.22	1.34	1.44	1.16	1.04	1.18	5.33	2.18	1.52	1.77
MISPT(125) [46]	1.58	1.80	0.58	0.99	0.74	0.93	0.73	0.45	0.41	3.60	0.88	0.68	1.11
MISPT(25) [46]	1.53	2.08	1.30	1.01	0.74	0.97	0.72	0.46	0.42	4.28	0.88	0.69	1.26
RLS [47]	1.34	1.28	0.82	1.37	0.90	1.31	0.95	0.96	0.73	3.01	1.28	0.85	1.23
WF+DFT [48]	1.23	1.26	0.72	0.98	0.75	0.91	0.67	0.91	0.54	2.61	0.94	0.98	1.04
SpaMA [49]	1.23	1.59	0.57	0.44	0.47	0.61	0.54	0.40	0.40	2.63	0.64	1.20	0.89
HEAL-T [50]	3.96	1.73	0.91	2.21	0.32	1.19	0.32	0.47	0.26	4.22	0.87	1.41	1.49
MURAD [51]	1.17	0.93	0.7	0.82	0.88	0.97	0.67	0.74	0.49	2.69	0.81	0.77	0.97
RLS+SD [52]	1.66	1.56	0.65	1.48	0.77	1.12	0.72	0.91	0.42	2.35	1.45	0.78	1.16
OSC-ANF [53]	1.95	1.89	1.64	2.10	1.25	1.62	1.23	1.72	1.27	2.98	1.49	1.37	1.71
EEMD+RLS [54]	1.70	0.84	0.56	1.15	0.77	1.06	0.63	0.53	0.52	2.56	1.05	0.91	1.02
MAC [55]	1.72	1.33	0.90	1.28	0.93	1.41	0.61	0.88	0.59	3.78	0.85	0.71	1.25
NLMS+AFT [56]	1.75	1.94	1.17	1.67	0.95	1.22	0.91	1.17	0.87	2.95	1.15	1.00	1.40

HSUM outperforms all the other algorithms because it depends on the harmonics of the PPG signals. The harmonics are suppressed by all the other algorithms by bandpass filtering.

This review article is confined to the dataset collected by Zhang *et al.*, because it is specific to the HR estimation when on treadmill. The other algorithms which are developed on datasets which are not available publicly are not discussed in this review [57, 58, 59, 60]. The algorithms for which the the performance across 12 subjects are not discussed is also excluded from the review since it confines the comparison across algorithms [61, 62]. PPG signals were also used to estimate other physiological parameters such as blood pressure and oxygen saturation [63, 64]. The details of the algorithms for computation of other physiological parameters are beyond the scope of this review. Heart-rate estimation from PPG acquired using other devices such as mobile phones and laptop cameras from other regions of interest for example forehead, ear is interesting and has its own unique challenge. However, its beyond the scope of this review here [65, 66].

Estimation of HR from PPG is validated using HR estimated from ECG which is the electrical activity of heart. Since, an error of 1 BPM is accepted clinically, three of the discussed algorithms have th potential to replace ECG for heart-rate estimation. PPG is widely used in clinic, hence it is safe to use. With advancement of wearable devices, acquisition of PPG signals is getting simpler than acquisition of ECG which has to be collected from a minimum of three electrodes [67]. Another important point to be noted is, with good denoising of PPG signals, other physiological parameters such as blood oxygen saturation, respiratory rate and anaesthesia monitoring can also be measured unlike those from ECG.

5 Conclusion

ECG is the gold standard for HR estimation. The algorithms discussed here are evaluated with HR estimated from ECG. Hence the evaluation method of these techniques are proven. The drawback of the current techniques are it is not validated across different PPG datasets. Since these algorithms developed are independent of the previous estimates, increase of the data acquisition in time may not affect the accuracy. However, the discussed algorithms are not robust to subjects during other tasks or patients data. The performance is expected to vary considerably. The monitoring of the HR is more essential in subjects with cardiac disorders. The robustness of the proposed algorithms across patient database is yet to be validated. Even though the numerous algorithms developed are real-time, porting these to the embedded device still remains a challenge.

Acknowledgement

This work was financially supported from the Tier 2 research grant funded by Ministry of Education in Singapore (ARC2/15: M4020238).

References

- [1] N. Selvaraj, A. Jaryal, et al., “Assessment of heart rate variability derived from finger-tip photoplethysmography as compared to electrocardiography,” *Journal of medical engineering & technology* 32(6), 479–484 (2008).
- [2] Y. Mendelson and B. D. Ochs, “Noninvasive pulse oximetry utilizing skin reflectance photoplethysmography,” *Biomedical Engineering, IEEE Transactions on* 35(10), 798–805 (1988).
- [3] H. Dubey, R. Kumaresan, and K. Mankodiya, “Harmonic sum-based method for heart rate estimation using PPG signals affected with motion artifacts,” *Journal of Ambient Intelligence and Humanized Computing* pp. 1–14 (2016).
- [4] T. Tamura, Y. Maeda, et al., “Wearable Photoplethysmographic Sensors Past and Present,” *Electronics* 3(2), 282–302 (2014).
- [5] J. Lee, W. Jung, et al., “Design of filter to reject motion artifact of pulse oximetry,” *Computer Standards & Interfaces* 26(3), 241–249 (2004).
- [6] H. Han, M.-J. Kim, and J. Kim, “Development of real-time motion artifact reduction algorithm for a wearable photoplethysmography,” in “Engineering in Medicine and Biology Society, 2007. EMBS 2007. 29th Annual International Conference of the IEEE,” pp. 1538–1541, IEEE (2007).
- [7] J. Yao and S. Warren, “A short study to assess the potential of independent component analysis for motion artifact separation in wearable pulse oximeter signals,” in “Engineering in Medicine and Biology Society, 2005. IEEE-EMBS 2005. 27th Annual International Conference of the,” pp. 3585–3588, IEEE (2005).

- [8] B. S. Kim and S. K. Yoo, “Motion artifact reduction in photoplethysmography using independent component analysis,” *Biomedical Engineering, IEEE Transactions on* 53(3), 566–568 (2006).
- [9] R. Krishnan, B. Natarajan, and S. Warren, “Two-stage approach for detection and reduction of motion artifacts in photoplethysmographic data,” *Biomedical Engineering, IEEE Transactions on* 57(8), 1867–1876 (2010).
- [10] Z. Zhang, Z. Pi, and B. Liu, “TROIKA: A general framework for heart rate monitoring using wrist-type photoplethysmographic signals during intensive physical exercise,” *IEEE Transactions on Biomedical Engineering* 62(2), 522–531 (2015).
- [11] R. Punchalard, C. Benjangkprasert, et al., “A robust variable step-size LMS-like algorithm for a second-order adaptive IIR notch filter for frequency detection,” in “Wireless Communications, 2001.(SPAWC’01). 2001 IEEE Third Workshop on Signal Processing Advances in,” pp. 232–234, IEEE (2001).
- [12] K. Chan and Y. Zhang, “Adaptive reduction of motion artifact from photoplethysmographic recordings using a variable step-size LMS filter,” in “Sensors, 2002. Proceedings of IEEE,” volume 2, pp. 1343–1346, IEEE (2002).
- [13] H. Han and J. Kim, “Artifacts in wearable photoplethysmographs during daily life motions and their reduction with least mean square based active noise cancellation method,” *Computers in biology and medicine* 42(4), 387–393 (2012).
- [14] P. Wei, R. Guo, et al., “A new wristband wearable sensor using adaptive reduction filter to reduce motion artifact,” in “Information Technology and Applications in Biomedicine, 2008. ITAB 2008. International Conference on,” pp. 278–281, IEEE (2008).

- [15] H. Fukushima, H. Kawanaka, et al., “Estimating heart rate using wrist-type photoplethysmography and acceleration sensor while running,” in “Engineering in Medicine and Biology Society (EMBC), 2012 Annual International Conference of the IEEE,” pp. 2901–2904, IEEE (2012).
- [16] L. B. Wood and H. H. Asada, “Active motion artifact reduction for wearable sensors using Laguerre expansion and signal separation,” in “Engineering in Medicine and Biology Society, 2005. IEEE-EMBS 2005. 27th Annual International Conference of the,” pp. 3571–3574, IEEE (2006).
- [17] M. J. Hayes and P. R. Smith, “A new method for pulse oximetry possessing inherent insensitivity to artifact,” *Biomedical Engineering, IEEE Transactions on* 48(4), 452–461 (2001).
- [18] Y.-s. Yan, C. C. Poon, and Y.-t. Zhang, “Reduction of motion artifact in pulse oximetry by smoothed pseudo Wigner-Ville distribution,” *Journal of NeuroEngineering and Rehabilitation* 2, 3 (2005).
- [19] M. Raghuram, K. V. Madhav, et al., “Evaluation of wavelets for reduction of motion artifacts in photoplethysmographic signals,” in “Information Sciences Signal Processing and their Applications (ISSPA), 2010 10th International Conference on,” pp. 460–463, IEEE (2010).
- [20] J. Y. A. Foo, “Comparison of wavelet transformation and adaptive filtering in restoring artefact-induced time-related measurement,” *Biomedical signal processing and control* 1(1), 93–98 (2006).
- [21] X. Sun, P. Yang, et al., “Robust heart beat detection from photoplethysmography interlaced with motion artifacts based on empirical mode decomposition,” in

- “Biomedical and Health Informatics (BHI), 2012 IEEE-EMBS International Conference on,” pp. 775–778, IEEE (2012).
- [22] E. Pinheiro, O. Postolache, and P. Girão, “Empirical mode decomposition and principal component analysis implementation in processing non-invasive cardiovascular signals,” *Measurement* 45(2), 175–181 (2012).
- [23] Y. Ye, W. He, et al., “A Robust Random Forest-Based Approach for Heart Rate Monitoring Using Photoplethysmography Signal Contaminated by Intense Motion Artifacts,” *Sensors* 17(2), 385 (2017).
- [24] B. Lee, J. Han, et al., “Improved elimination of motion artifacts from a photoplethysmographic signal using a Kalman smoother with simultaneous accelerometry,” *Physiological measurement* 31(12), 1585 (2010).
- [25] M. P. Tarvainen, S. D. Georgiadis, et al., “Time-varying analysis of heart rate variability signals with a Kalman smoother algorithm,” *Physiological measurement* 27(3), 225 (2006).
- [26] K. Nakajima, T. Tamura, and H. Miike, “Monitoring of heart and respiratory rates by photoplethysmography using a digital filtering technique,” *Medical engineering & physics* 18(5), 365–372 (1996).
- [27] H. H. Asada, H.-H. Jiang, and P. Gibbs, “Active noise cancellation using MEMS accelerometers for motion-tolerant wearable bio-sensors,” in “Engineering in Medicine and Biology Society, 2004. IEMBS’04. 26th Annual International Conference of the IEEE,” volume 1, pp. 2157–2160, IEEE (2004).

- [28] M. T. Islam, S. T. Ahmed, et al., “Cascade and Parallel Combination (CPC) of Adaptive Filters for Estimating Heart Rate During Intensive Physical Exercise from Photoplethysmographic Signal,” *Healthcare Technology Letters* (2017).
- [29] F. Peng, H. Liu, and W. Wang, “A comb filter based signal processing method to effectively reduce motion artifacts from photoplethysmographic signals,” *Physiological measurement* 36(10), 2159 (2015).
- [30] F. Wadehn, D. Carnal, and H.-A. Loeliger, “Estimation of heart rate and heart rate variability from pulse oximeter recordings using localized model fitting,” in “Engineering in Medicine and Biology Society (EMBC), 2015 37th Annual International Conference of the IEEE,” pp. 3815–3818, IEEE (2015).
- [31] F. Peng, Z. Zhang, et al., “Motion artifact removal from photoplethysmographic signals by combining temporally constrained independent component analysis and adaptive filter,” *Biomedical engineering online* 13(1), 1 (2014).
- [32] Y. Ye, Y. Cheng, et al., “Combining Nonlinear Adaptive Filtering and Signal Decomposition for Motion Artifact Removal in Wearable Photoplethysmography,” *IEEE Sensors Journal* 16(19), 7133–7141 (2016).
- [33] Z.-H. Zhang, J. Liu, et al., “A new framework to extract heart rate information from photoplethysmographic (PPG) signals with strong motion artifacts,” in “TENCON 2015-2015 IEEE Region 10 Conference,” pp. 1–4, IEEE (2015).
- [34] E. Grisan, G. Cantisani, et al., “A supervised learning approach for the robust detection of heart beat in plethysmographic data,” in “Engineering in Medicine and Biology Society (EMBC), 2015 37th Annual International Conference of the IEEE,” pp. 5825–5828, IEEE (2015).

- [35] A. Baca, G. Biagetti, et al., “CARMA: A robust motion artifact reduction algorithm for heart rate monitoring from PPG signals,” in “Signal Processing Conference (EU-SIPCO), 2015 23rd European,” pp. 2646–2650, IEEE (2015).
- [36] Y. Zhang, B. Liu, and Z. Zhang, “Combining ensemble empirical mode decomposition with spectrum subtraction technique for heart rate monitoring using wrist-type photoplethysmography,” *Biomedical Signal Processing and Control* 21, 119–125 (2015).
- [37] G. Frigo, M. Fabris, et al., “Efficient tracking of heart rate under physical exercise from photoplethysmographic signals,” in “Research and Technologies for Society and Industry Leveraging a better tomorrow (RTSI), 2015 IEEE 1st International Forum on,” pp. 306–311, IEEE (2015).
- [38] B. Sun and Z. Zhang, “Photoplethysmography-based heart rate monitoring using asymmetric least squares spectrum subtraction and bayesian decision theory,” *IEEE Sensors Journal* 15(12), 7161–7168 (2015).
- [39] M. Farhadi, M. B. Mashhadi, et al., “RealTime Heart Rate Monitoring Using Photoplethysmographic (PPG) Signals During Intensive Physical Exercises,” *bioRxiv* p. 092627 (2016).
- [40] B. Sun, H. Feng, and Z. Zhang, “A new approach for heart rate monitoring using photoplethysmography signals contaminated by motion artifacts,” in “2016 IEEE International Conference on Acoustics, Speech and Signal Processing (ICASSP),” pp. 809–813, IEEE (2016).

- [41] Z. Zhang, “Photoplethysmography-based heart rate monitoring in physical activities via joint sparse spectrum reconstruction,” *IEEE Transactions on Biomedical Engineering* 62(8), 1902–1910 (2015).
- [42] Z. Zhang, Z. Pi, and B. Liu, “TROIKA: A General Framework for Heart Rate Monitoring Using Wrist-Type Photoplethysmographic (PPG) Signals During Intensive Physical Exercise.” *IEEE transactions on bio-medical engineering* 9294(c), 1–10 (2014), URL <http://www.ncbi.nlm.nih.gov/pubmed/25252274>.
- [43] J. Xiong, L. Cai, et al., “Spectral matrix decomposition-based motion artifacts removal in multi-channel PPG sensor signals,” *IEEE Access* 4, 3076–3086 (2016).
- [44] D. Zhao, Y. Sun, et al., “SFST: A robust framework for heart rate monitoring from photoplethysmography signals during physical activities,” *Biomedical Signal Processing and Control* 33, 316–324 (2017).
- [45] T. Schäck, C. Sledz, et al., “A new method for heart rate monitoring during physical exercise using photoplethysmographic signals,” in “Signal Processing Conference (EUSIPCO), 2015 23rd European,” pp. 2666–2670, IEEE (2015).
- [46] N. K. L. Murthy, P. C. Madhusudana, et al., “Multiple spectral peak tracking for heart rate monitoring from photoplethysmography signal during intensive physical exercise,” *IEEE Signal Processing Letters* 22(12), 2391–2395 (2015).
- [47] S. T. Ahamed and M. T. Islam, “An efficient method for heart rate monitoring using wrist-type photoplethysmographic signals during intensive physical exercise,” in “Informatics, Electronics and Vision (ICIEV), 2016 5th International Conference on,” pp. 863–868, IEEE (2016).

- [48] A. Temko, “Estimation of heart rate from photoplethysmography during physical exercise using Wiener filtering and the phase vocoder,” in “2015 37th Annual International Conference of the IEEE Engineering in Medicine and Biology Society (EMBC),” pp. 1500–1503, IEEE (2015).
- [49] S. Salehizadeh, D. Dao, et al., “A novel time-varying spectral filtering algorithm for reconstruction of motion artifact corrupted heart rate signals during intense physical activities using a wearable photoplethysmogram sensor,” *Sensors* 16(1), 10 (2015).
- [50] J. M. M. Torres, A. Ghosh, et al., “Heal-T: An efficient PPG-based heart-rate and IBI estimation method during physical exercise,” in “Signal Processing Conference (EUSIPCO), 2016 24th European,” pp. 1438–1442, IEEE (2016).
- [51] S. Chowdhury, R. Hyder, et al., “Real Time Robust Heart Rate Estimation from Wrist-type PPG Signals Using Multiple Reference Adaptive Noise Cancellation,” *IEEE Journal of Biomedical and Health Informatics* (2016).
- [52] Y. Ye, Y. Cheng, et al., “Combining Nonlinear Adaptive Filtering and Signal Decomposition for Motion Artifact Removal in Wearable Photoplethysmography,” *IEEE Sensors Journal* 16(19), 7133–7141 (2016).
- [53] S. Fallet and J.-M. Vesin, “Adaptive frequency tracking for robust heart rate estimation using wrist-type photoplethysmographic signals during physical exercise,” in “2015 Computing in Cardiology Conference (CinC),” pp. 925–928, IEEE (2015).
- [54] E. Khan, F. Al Hossain, et al., “A robust heart rate monitoring scheme using photoplethysmographic signals corrupted by intense motion artifacts,” *IEEE Transactions on Biomedical Engineering* 63(3), 550–562 (2016).

- [55] M. B. Mashhadi, E. Asadi, et al., “Heart Rate Tracking using Wrist-Type Photoplethysmographic (PPG) Signals during Physical Exercise with Simultaneous Accelerometry,” *IEEE Signal Processing Letters* 23(2), 227–231 (2016).
- [56] S. Fallet and J.-M. Vesin, “Robust heart rate estimation using wrist-type photoplethysmographic signals during physical exercise: an approach based on adaptive filtering,” *Physiological Measurement* 38(2), 155 (2017).
- [57] A. Alqaraawi, A. Alwosheel, and A. Alasaad, “Towards efficient heart rate variability estimation in artifact-induced Photoplethysmography signals,” in “Electrical and Computer Engineering (CCECE), 2016 IEEE Canadian Conference on,” pp. 1–6, IEEE (2016).
- [58] A. Alqaraawi, A. Alwosheel, and A. Alasaad, “Heart rate variability estimation in photoplethysmography signals using Bayesian learning approach,” *Healthc Technol Lett* 3, 136–142 (2016).
- [59] S. A. Kazmi, S. Khan, et al., “Spectrum analysis of physiological signals of human activities,” in “Emerging Technologies (ICET), 2015 International Conference on,” pp. 1–6, IEEE (2015).
- [60] Y. Wang, Z. Liu, and B. Dong, “Heart rate monitoring from wrist-type PPG based on singular spectrum analysis with motion decision,” in “Engineering in Medicine and Biology Society (EMBC), 2016 IEEE 38th Annual International Conference of the,” pp. 3511–3514, IEEE (2016).
- [61] P. Mullan, C. M. Kanzler, et al., “Unobtrusive heart rate estimation during physical exercise using photoplethysmographic and acceleration data,” in “Engineering in

- Medicine and Biology Society (EMBC), 2015 37th Annual International Conference of the IEEE,” pp. 6114–6117, IEEE (2015).
- [62] T. Hayashi and T. Ooi, “Estimation of Heart Rate during Exercise from a Photoplethysmographic Signal Considering Exercise Intensity,” *Sensors and Materials* 28(4), 341–348 (2016).
- [63] Y. Zheng, C. C. Poon, et al., “Pulse Arrival Time Based Cuff-Less and 24-H Wearable Blood Pressure Monitoring and its Diagnostic Value in Hypertension,” *Journal of medical systems* 40(9), 195 (2016).
- [64] J. Allen, “Photoplethysmography and its application in clinical physiological measurement,” *Physiological measurement* 28(3), R1 (2007).
- [65] D. Jarchi and A. J. Casson, “Description of a Database Containing Wrist PPG Signals Recorded during Physical Exercise with Both Accelerometer and Gyroscope Measures of Motion,” *Data* 2(1), 1 (2016).
- [66] L. Pu, P. J. Chacon, et al., “Novel tailoring algorithm for abrupt motion artifact removal in photoplethysmogram signals,” *Biomedical Engineering Letters* pp. 1–6 (2017).
- [67] A. Standard, “Z136. 1. American national standard for the safe use of lasers. American National Standards Institute,” *Inc., New York* (1993).

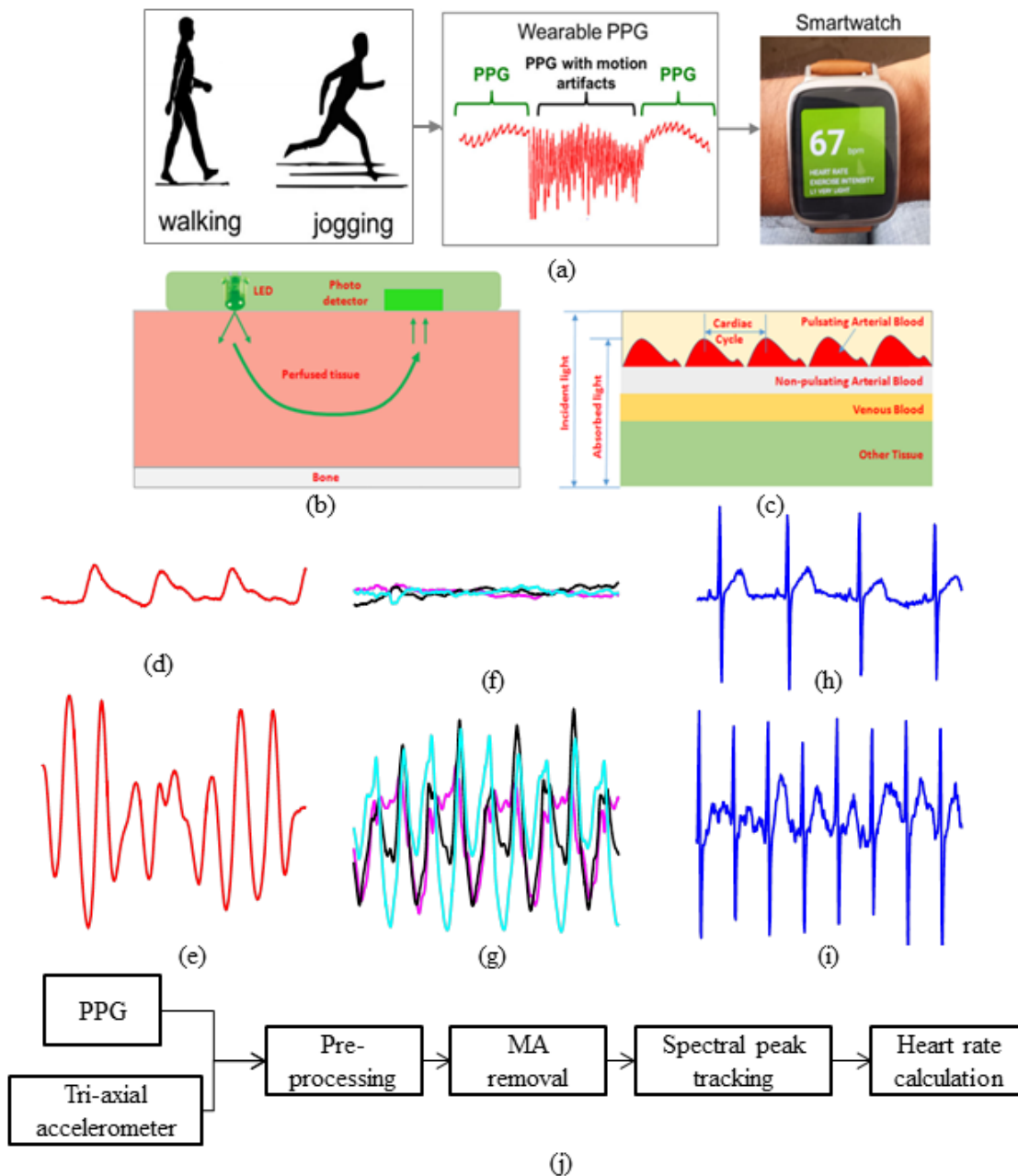


Figure 1: (a) Acquisition of PPG signal [3], (b) Illustration source and detector [3], (c) Components of PPG signal [3], (d) Sample PPG signal for 3 seconds, (e) PPG signal with MA, (f) MA from tri-axial accelerometer during rest, (g) MA from tri-axial accelerometer during exercise, (h) ECG signal during rest, (i) ECG signal during motion, (j) Block-diagram of steps involved in HR estimation. All figures are reproduced with permission.

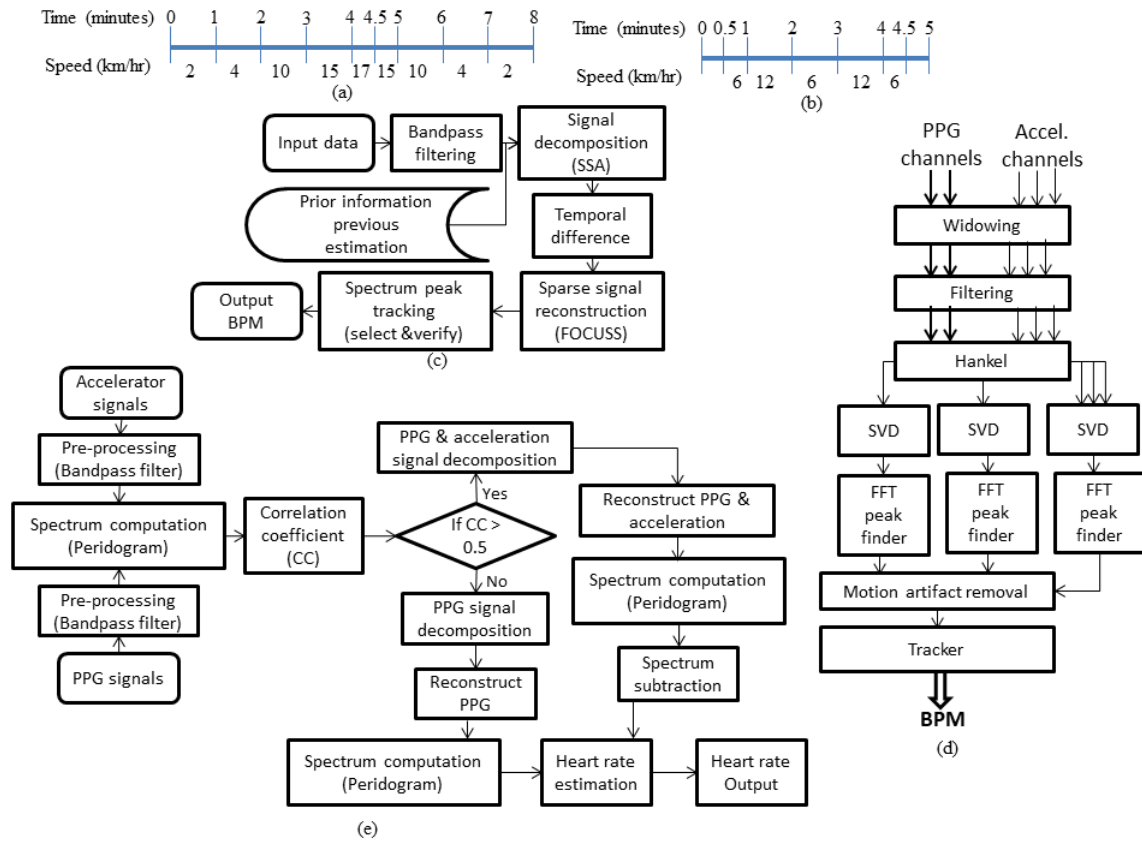


Figure 2: (a) Representation of dataset 1 (b) Representation of dataset 2 (c) TROIKA framework [10], block diagram of (d) CARMA [35] and, (e) Empirical mode decomposition [36].

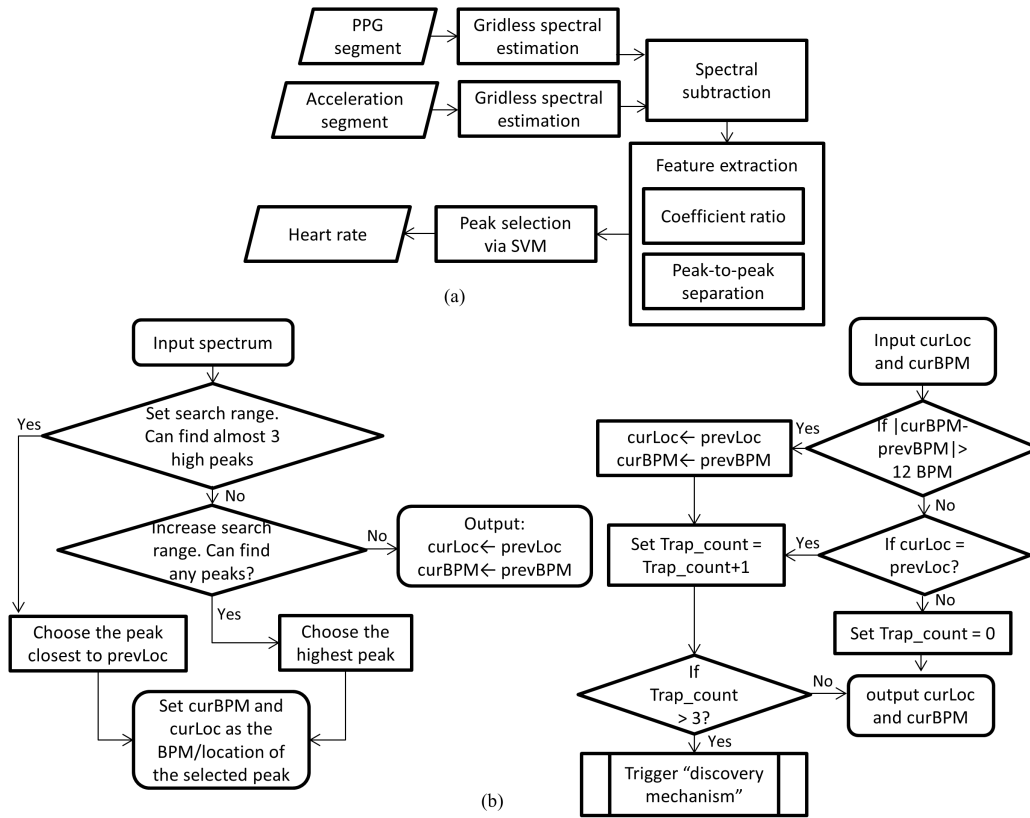


Figure 3: (a) Block diagram of GRESS [40] and (b) flow-chart of JOSS [41].

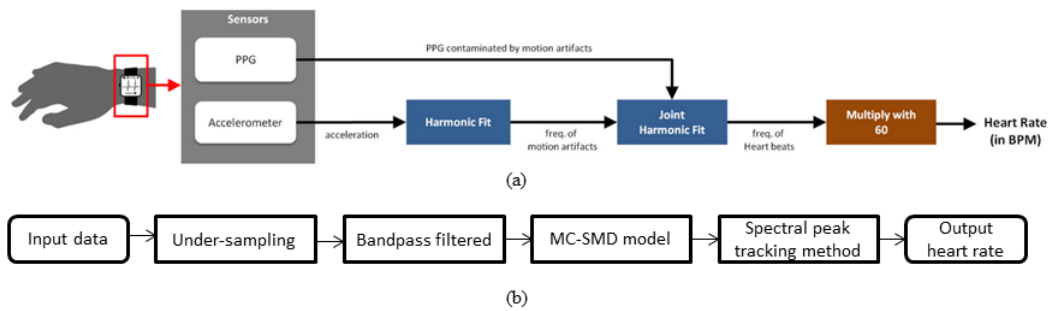


Figure 4: Block diagram of (a) HSUM [3] (reproduced with permission) and (b) MC+SMD [43].

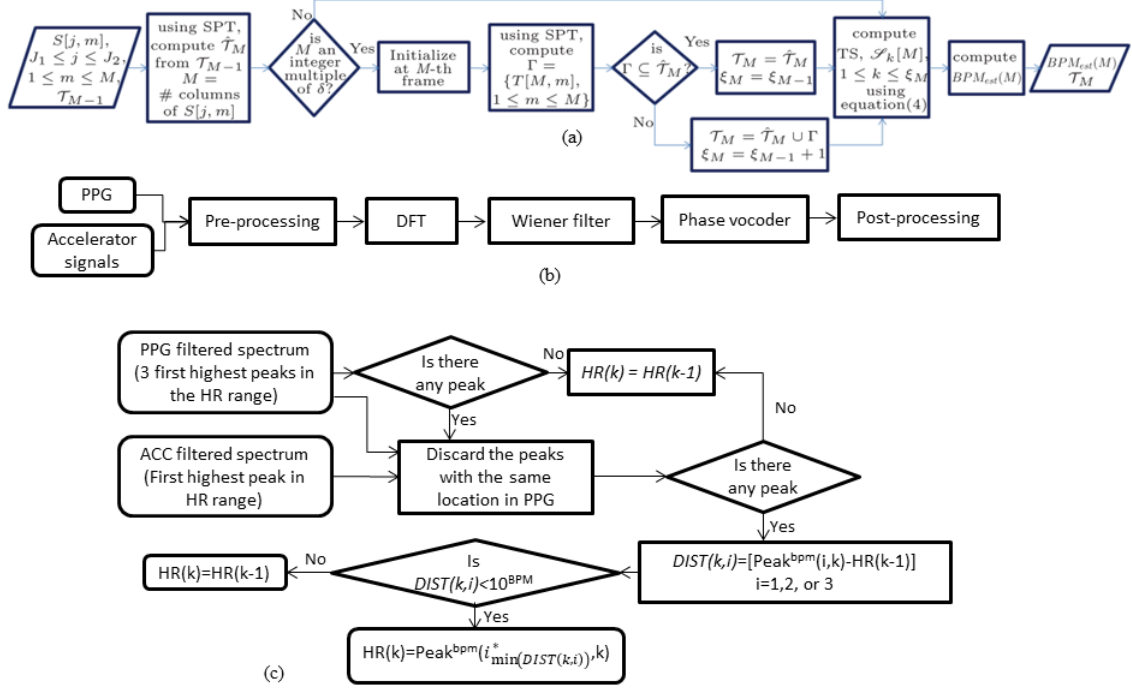


Figure 5: (a) Flow-chart of MISPT [46], (b) block diagram of WF+PV [48], (c) flow-chart of SpaMA [49].

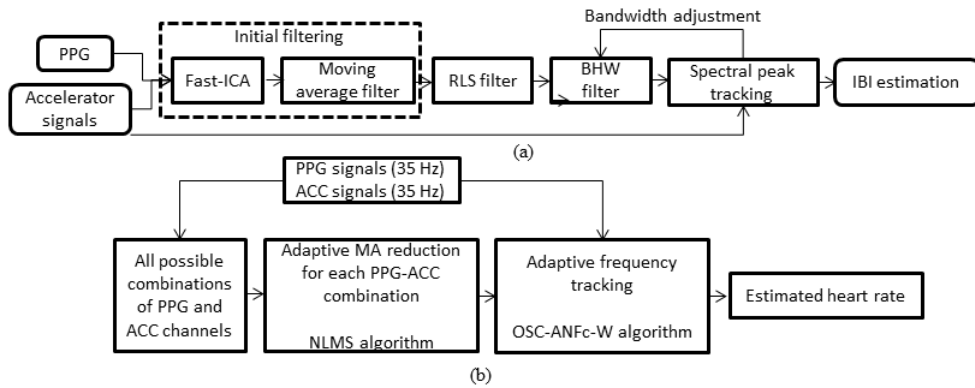


Figure 6: Block diagram of (a) HEAL-T [50] and (b) NLMS+AFT [56].